Environmental Science and Pollution Research (2024) 31:30059–30071
https://doi.org/10.1007/s11356-024-33239-4

RESEARCH ARTICLE

Study on the performance and mechanism of cobaltous ion removal from water by a high-efficiency strontium-doped hydroxyapatite adsorbent

Zongqiang Zhu[1,2,3] · Shuangshuang Liu[1] · Yinian Zhu[1,2] · Hao He[1] · Jun Zhang[1] · Xiaoxin Mo[1,2] · Shen Tang[1,2] · Yinming Fan[1,2] · Lihao Zhang[1,2] · Xiaobin Zhou[1,2,4]

Received: 10 December 2023 / Accepted: 3 April 2024 / Published online: 10 April 2024

Abstract

In this study, a high-efficiency strontium-doped hydroxyapatite (Sr-HAP) adsorbent was synthesized by a sol-gel method for removing cobaltous ions (Co(II)) from water. The effects of adsorbent dose, initial solution pH, initial Co(II) concentration and temperature on the removal performance of Co(II) were investigated. Experimental results indicated that the optimum Sr-HAP dose was 0.30 g/50 mL solution, the Sr-HAP adsorbent could effectively remove Co(II) in a wide pH range of 3–8. Increasing temperature was conducive to the adsorption, and the maximum Co(II) adsorption capacity by Sr-HAP reached 48.467 mg/g at 45 °C. The adsorption of Co(II) followed the pseudo-second-order kinetic model, indicating that the Co(II) adsorption by Sr-HAP was attributed mainly to chemisorption. The isothermal adsorption results showed that at lower Co(II) equilibrium concentration, the Langmuir model fitted the data better than the Freundlich model but opposite at higher Co(II) equilibrium concentration. Therefore, the adsorption of Co(II) was a process from monolayer adsorption to multilayer adsorption with the increase of the Co(II) equilibrium concentration. The diffusion analysis of Co(II) to Sr-HAP indicated that the internal diffusion and surface adsorption were the rate-controlled steps of Co(II) adsorption. Thermodynamic study demonstrated that the Co(II) adsorption process was spontaneous and endothermic. The mechanism study revealed that in addition to chemisorption, Sr-HAP also removed Co(II) ions from water via ion exchange and surface complexation.

Keywords Strontium-doped hydroxyapatite · Cobaltous ions · Kinetics · Thermodynamics · Mechanism

Introduction

Cobalt (Co) is an important metal and has been widely used in the production of batteries, alloys, and other products (Zhong et al. 2018). In the above industries, Co-containing wastewater has been produced in quantity. Co exists mainly in the form of cobaltous ion (Co(II)), which has very serious cytotoxicity and genotoxicity (Li et al. 2023), and is a kind of carcinogen that is very harmful to human health. In addition, its harm to animals, plants and even the whole ecosystem has caused widespread concern (Bhawna and Kirandeep 2023; Kosiorek 2019). For this reason, the World Health Organization stipulates that the maximum allowable concentration of Co(II) in drinking water is 0.05 mg/L. Therefore, it is crucial to remove Co(II) before Co-containing wastewater is discharged.

Various technologies have been employed for removing Co(II) from wastewater, including precipitation (Joo et al. 2020), coagulation/flocculation (Punia et al. 2022),

Responsible Editor: Tito Roberto Cadaval Jr

✉ Xiaobin Zhou
zhouxiaobin@glut.edu.cn

[1] Collaborative Innovation Center for Water Pollution Control and Water Safety in Karst Area, Guilin University of Technology, Guilin 541004, China

[2] The Guangxi Key Laboratory of Theory and Technology for Environmental Pollution Control, Guilin University of Technology, Guilin 541004, China

[3] Technical Innovation Center of Mine Geological Environmental Restoration Engineering in Southern Karst Area, Nanning 530022, China

[4] College of Environmental Science and Engineering, Guilin University of Technology, Guilin 541004, Guangxi, China

ion exchange, membrane separation (Li et al. 2021), and adsorption (Che et al. 2022; Liao et al. 2022). Among them, adsorption has attracted extensive attention, which is low-cost and easy to operate for treating heavy metal-containing wastewater. Common adsorbents include montmorillonite (Mao et al. 2021), bentonite (Pourshadlou et al. 2023), silica (Cherif et al. 2023) and activated carbon (Chakraborty et al. 2022). The unique pore structure of these materials determines their good adsorption properties for heavy metals. However, the raw adsorbents typically take several hours or longer to achieve adsorption equilibrium due to their small specific surface area, irregular pore channel distribution, and insufficient capacity (Mahar et al. 2023). Therefore, it is crucial to develop new adsorbents with higher adsorption capacity and faster adsorption rate.

Hydroxyapatite (HAP) is a brand-new class of functional material that is ecologically friendly. Its crystal structure belongs to the hexagonal system and its unit cell contains 10 Ca^{2+}, 6 PO_4^{3-} and 2 OH^- ($Ca_{10}(PO_4)_6(OH)_2$). The unique cell structure of HAP allows it to undergo ion exchange, surface reaction or surface precipitation with numerous cations and anions. Iconaru et al. (2018) found that hydroxyapatite nanopowders (N-HAP) showed good adsorption of Pb^{2+}, which was due to the coupling of the positive charge of Pb^{2+} with the negative charge on N-HAP. Leyva et al. (2001) used HAP to remove Sb^{3+} from water and demonstrated that the rapid surface reaction between HAP and Sb^{3+} enabled the efficient elimination of Sb^{3+}. To further improve the properties of HAP, the effective approach of metal doping modification could be used. The modified HAP has been proved to possess significantly greater volumes, specific surfaces, and active sites than the raw HAP. Accordingly, the modified HAP had a much higher adsorption capacity (Metwally et al. 2017; Hokkanen et al. 2014). Recently, strontium (Sr)-doped HAP had been proposed to remove heavy metal ions from wastewater. Since the atomic radius between Sr and Ca is different (Singh et al. 2023), the introduction of Sr changed the characteristic properties of HAP, such as the increase of pore volume, specific surface area, stability and activity, which was conducive to the adsorption process. However, the information on the Sr-doped HAP is still limited, and the synthesis of Sr-doped HAP with high efficiency is crucial. Moreover, few studies on Sr-doped HAP used for the Co(II) removal from wastewater have been reported in the open literature.

In this study, an efficient Sr-doped HAP adsorbent was synthesized via a facile sol-gel method and then used for the uptake of Co(II) from water. The effects of adsorbent dose, initial solution pH, and initial Co(II) concentration on the Co(II) removal were investigated. Moreover, the thermodynamic and kinetic behavior of Co(II) adsorption by Sr-doped HAP were also studied. Based on the experimental results and characterization analysis, the removal mechanism of Co(II) by the Sr-HAP adsorbent was elaborated. The results of this study may provide key data and theoretical basis for the Co removal by the new Sr-doped HAP adsorbent.

Materials and methods

Experimental materials

Strontium nitrate ($Sr(NO_3)_2$) and calcium nitrate tetrahydrate ($Ca(NO_3)_2{\cdot}4H_2O$) were bought from Xilong Chemical Co., Ltd. Diammonium phosphate ($(NH_4)_2HPO_4$), sodium hydroxide (NaOH), sodium dihydrogen phosphate (Na_2HPO_4), sodium chloride (NaCl), cobalt nitrate hexahydrate ($Co(NO_3)_26H_2O$), nitric acid (HNO_3), and ammonia ($NH_3{\cdot}H_2O$) were purchased from Shanghai Aladdin Biochemical Technology Co., Ltd. The above reagents are all analytically pure except for the specified purity. The experimental water is ultrapure.

Preparation of Sr-HAP

Firstly, 0.2 mol/L $Ca(NO_3)_2{\cdot}4H_2O$, $Sr(NO_3)_2$, and Na_2HPO_4 solutions were prepared, respectively. A certain amount of $Sr(NO_3)_2$ and $Ca(NO_3)_2{\cdot}4H_2O$ solutions were mixed according to the molar ratio $Sr/(Ca+Sr)=0.5$. Na_2HPO_4 was then added to the above mixture according to $(Sr+Ca)/P=1.67$. Meanwhile, $NH_3{\cdot}H_2O$ was added to adjust the pH value to 10 ~ 11, with stirring for 2 min, followed by 30 min of magnetic stirring. Whereafter, the mixture was aged for 24 h in a water bath at 50 °C. The precipitate was centrifuged at 4000 rpm for 5 min. The obtained precipitate was washed thrice with ultrapure water to neutrality. After washing by anhydrous ethanol, the product was dried at 80 °C in an oven for 24 h. Finally, the obtained materials, namely, the Sr-HAP adsorbent, was ground with 100 mesh sieve and preserved in a glass desiccator.

Characterizations

The microscopic morphology of the adsorbent was examined using energy dispersive spectroscopy (EDS) and field emission scanning electron microscopy (SEM) (JSM-6380LV, Japan). The composition and structure of the material were ascertained using a Fourier transform infrared absorption spectrometer (FTIR, 470 Thermonico Coolie, USA), an X-ray diffractometer (XRD, X 'Pert PRO, Panaco, Netherlands), and an X-ray photoelectron spectroscopy analyzer (XPS, ESCALAB 250 Xi, Semmerfeld, USA). The specific surface area and pore size were analyzed using a specific surface and porosity analyzer (NOVA1000e, Quantanchrome, USA).

Adsorption experiments

For a typical test, a certain amount of Sr-HAP was added to 50 mL simulated Co(II)-containing wastewater, which was put in a centrifuge tube (100 mL). The tube was then placed in a shaking bath at 150 r/min. At regular intervals, the mixture was centrifuged to obtain clear solution, which was further filtrated using a 0.22-μm fiber filter. The filtered sample was detected using an inductively coupled plasma optical emission spectrometer (ICP-OES) to determine the residual Co(II) concentration.

The effects of different factors on the Co(II) removal, including adsorbent dosage (0.05–0.50 g/50 mL), solution pH (1–10), initial Co(II) concentration (10–500 mg/L), and temperature (25–45 °C), were investigated. The solution was adjusted by 0.01 mol/L KOH or 0.01 mol/L HNO_3 to obtain the desired pH value.

Results and discussion

Characterizations

Figure 1a–b presents the XRD patterns of the Sr-HAP adsorbent before and after treating different solutions that containing different Co(II) concentrations. It was observed that the diffraction peaks of the synthesized Sr-HAP were consistent with those of the standard PDF card (01-074-0565) of HAP, indicating that Sr doping had no effect on the structure of HAP, and Sr-HAP maintained the hexagonal crystal structure as HAP did (Fig. 1a). After treating the Co(II)-containing solution, the XRD pattern of the used Sr-HAP had no obvious change, even if the Co(II) concentration increased to 500 mg/L. This result indicted the hexagonal crystal structure of Sr-HAP after Co(II) adsorption retained unchanged. However, the positions of the characteristic peaks of (211) and (002) slightly shifted

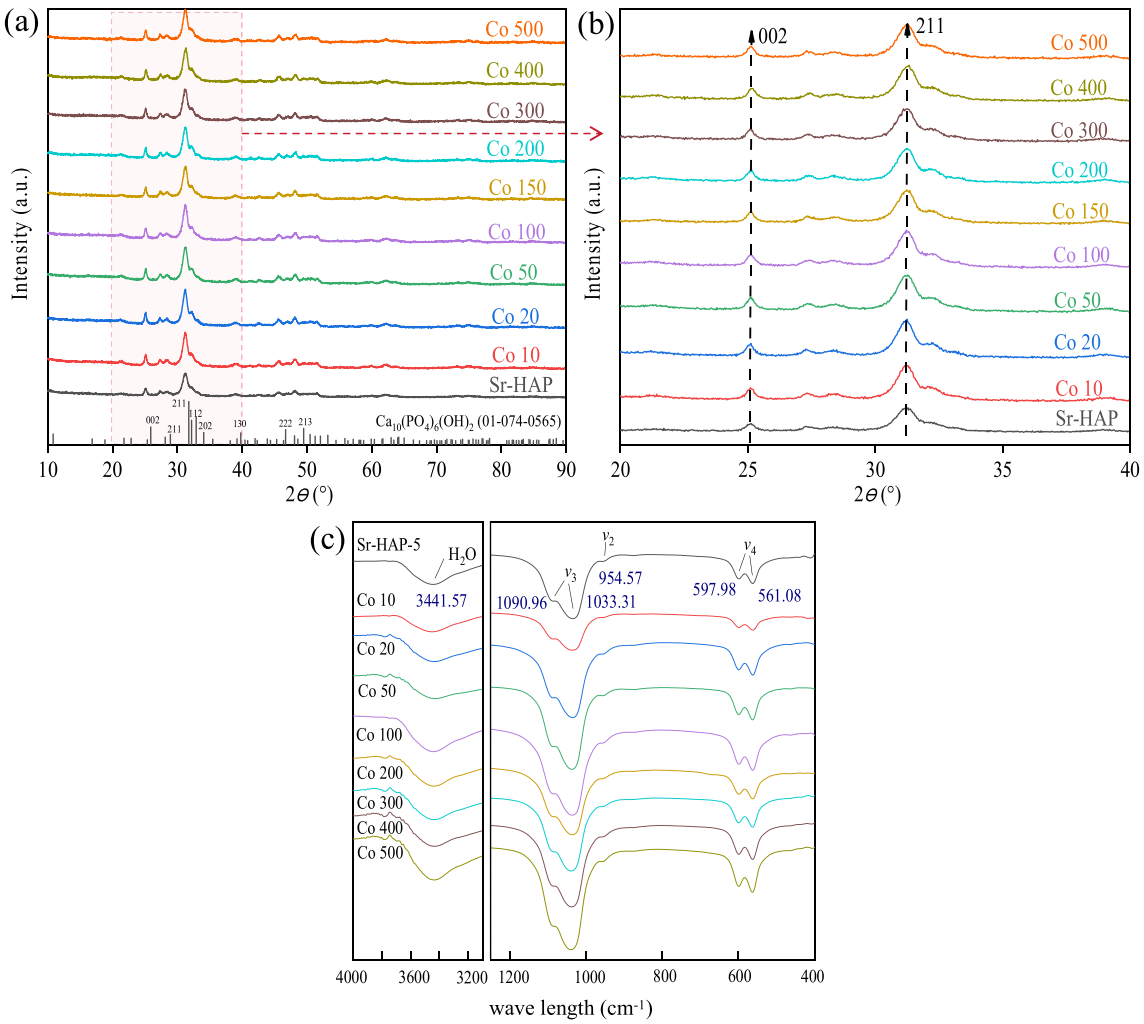

Fig. 1 **a** and **b** XRD patterns of Sr-HAP, **c** FT-IR spectra of Sr-HAP

to higher angles as the Co(II) concentration increased (Fig. 1b), which was due to the reduction of lattice parameters. By calculation, the lattice parameters of a = b and c dropped from 9.580 Å and 7.070 Å (Co-10) to 9.428 Å and 6.876 Å (Co-500), respectively. This change might relate to the ion exchange between Sr or Ca ions in Sr-HAP and Co(II) ions. The ionic radius of Co(II) is 0.72 Å, while those of Sr and Ca ions are 1.12 and 0.99 Å, respectively. Accordingly, the unit lattice parameter decreased when Co(II) ions replaced Sr or Ca ions in the Sr-HAP adsorbent (Liu et al. 2013). The higher is the Co(II) concentration, the more Sr or Ca ions were replaced, resulting more significant shift of the characteristic peaks.

The FT-IR spectra of the virgin and used Sr-HAP samples are shown in Fig. 1c. It was observed that the spectra of the used Sr-HAP presented the same characteristic peaks as did the virgin Sr-HAP, indicating that the functional groups of Sr-HAP did not changed after the Co(II) treatment. Interestingly, the peak intensity of the tensile vibration of PO_4^{3-} at 1033.31 (v_3) and 563.62 cm^{-1} (v_4) gradually increased as the treated Co(II) concentration increased. It might be attributed to that a large number of Co(II) ions were adsorbed and reacted with Sr-HAP, affecting the vibration of the PO_4^{3-} group (Shamrai et al. 2014).

Figure 2 presents the SEM and EDS images of the virgin and used Sr-HAP samples. Like the unused Sr-HAP, the morphology of the used Sr-HAP still kept the granular rod-like structure, but the particle agglomeration become serious, the porosity between the particles was reduced, and the material surface became rough. Combined with the FT-IR results, this penomenon might be that PO_4^{3-} in Sr-HAP reacted with Co(II) to form the $Co_{10}(PO_4)_6OH_2$ compound, which deposited on the surface of Sr-HAP (Zhu et al. 2018, 2022). The EDS results verified the presence of O, P, Ca and Sr in Sr-HAP before adsorption, and Co was introduced into Sr-HAP after adsorption. It was observed that the atomic percentages of O and P changed slightly before and after Co(II) adsorption. The slight change might be caused by Co(II) being adsorbed on the Sr-HAP adsorbent. Before Co(II) adsorption, the atomic ratio of (Sr + Ca)/P was 1.59, which decreased to 1.42 after Co(II) adsorption. Meanwhile, the atomic ratio of Sr/Ca did not changed significantly. This implied both Sr(II) and Ca(II) in Sr-HAP could undergo ion exchange with Co(II), and the exchange abilities of Sr(II) and Ca(II) with Co(II) were comparable.

N_2 adsorptions-desorption test was conducted to determine the specific surface area and pore size of Sr-HAP. As shown in Fig. S1. the adsorption-desorption isotherm curve

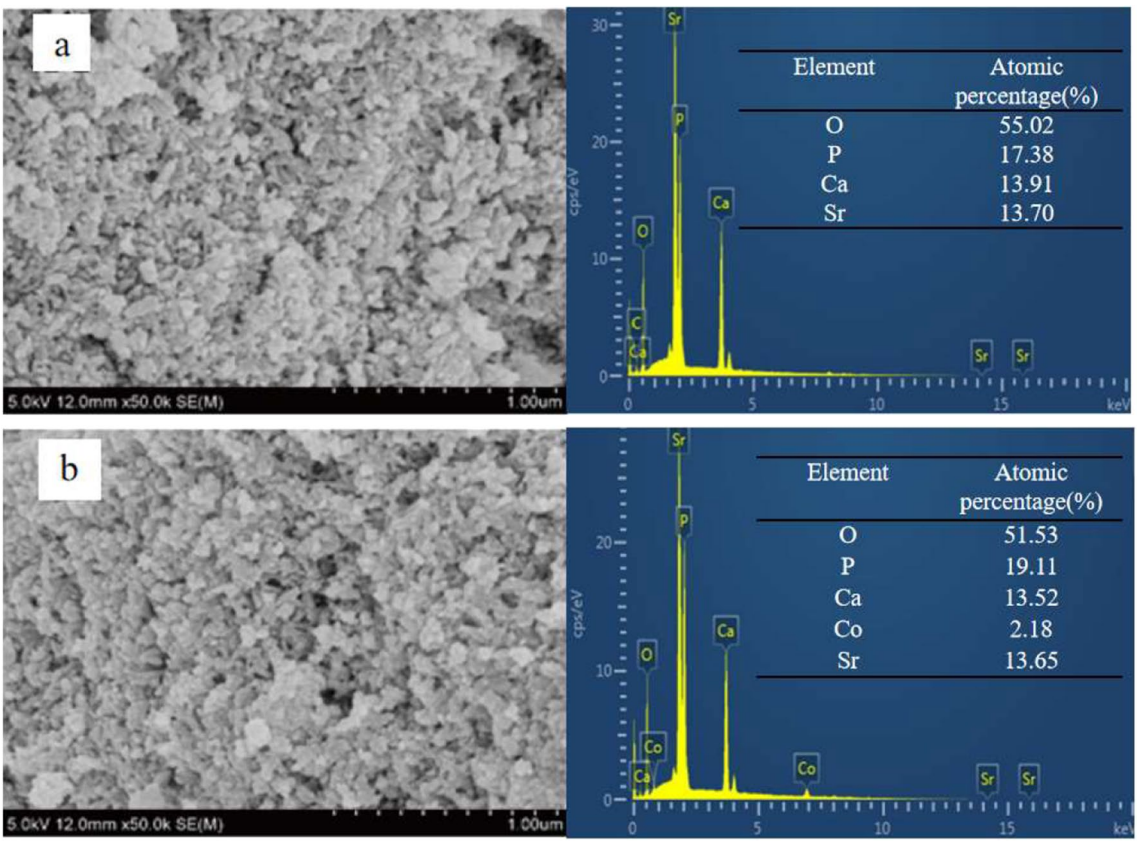

Fig. 2 SEM and EDS of Sr-HAP. **a** before and **b** after Co(II) adsorption

of Sr-HAP conformed to the type IV profile and showed a H_3 type hysteresis loop, indicating that Sr-HAP was a porous material with open wedge holes at both ends (ALOthman 2012). The specific surface area of Sr-HAP was calculated to be 115.121 m^2/g, which was 11.1% higher than that of HAP (Zhu et al. 2022). Fig. S2 shows the pore size distribution of Sr-HAP. It was observed that the pore size of Sr-HAP was mainly distributed in the range of 2–50 nm, which indicated that Sr-HAP belonged to a mesoporous material and was expected to have great adsorption capacities for heavy metal ions.

The chemical composition of the virgin and used Sr-HAP samples was examined using XPS measurement. In the wide scan spectra of the virgin and used Sr-HAP samples, the main characteristic peaks of Sr, P, Ca, and O elements were presented (Fig. 3a). Interestingly, the emerging characteristic peak of Co element was observed in the spectrum of the used Sr-HAP, indicating that Co(II) was

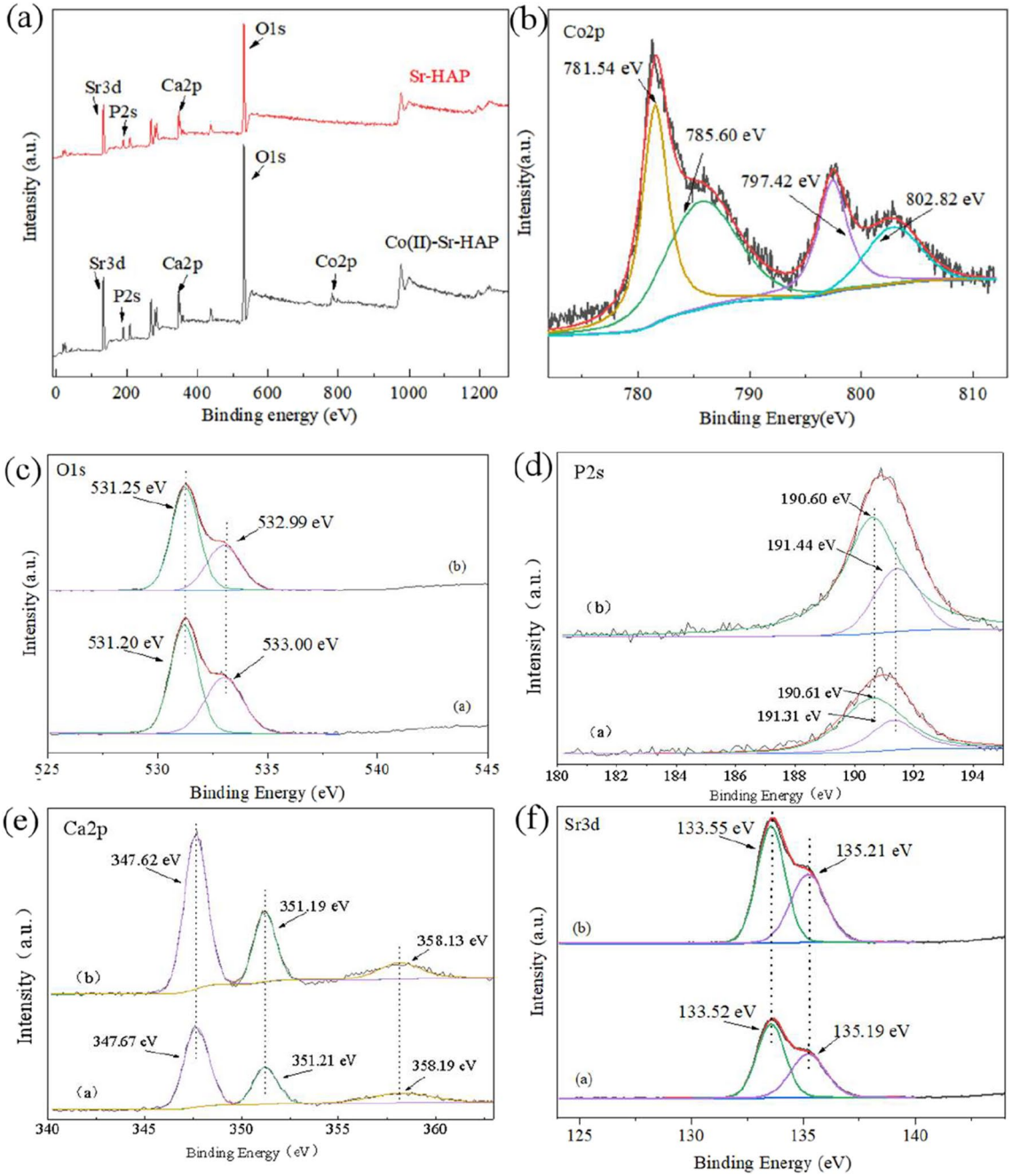

Fig. 3 **a** Wide scan XPS spectra of Sr-HAP before and after Co(II) adsorption; **b–f** High-resolution XPS spectra of Co2p, O1s, P2s, Ca2p, and Sr3d, respectively

adsorbed on the Sr-HAP's surface. The binding energy of $Co2p_{1/2}$ at 802.02 and 797.42 eV and $Co2p_{3/2}$ at 782.1 and 785.60 eV could be assigned to the cobaltous oxide (Chen et al. 2017; Li et al. 2019; Zhang et al. 2019) (Fig. 3b), indicating that there was no redox reaction during Co(II) adsorption. Figure 3c–f presents the high-resolution maps of O, P, Ca and Sr elements in Sr-HAP. The binding energy of these elements in the used Sr-HAP had no obvious change compared to that in the virgin Sr-HAP, but the associated peak intensity and area changed. For O1s, the relative peak intensity at about 531.20 eV decreased after Co(II) adsorption, which indicated the binding of Co and O in the form of Co-OOH (Deliyanni et al. 2006). The binding energy of P2s at 191.31 eV shifted to 191.44 eV after Co(II) adsorption, which may be caused by the decrease in the electronic density around the phosphorus atoms on the Sr-HAP's surface (Campisi et al. 2021), indicating that some PO_4^{3-} groups were involved in Co(II) adsorption. After the adsorption of Co(II), the binding energy of Ca2p and Sr3d basically did not change, indicating that Ca and Sr existed in the Co-loaded Sr-HAP in the same binding mode as they did in the pristine Sr-HAP.

Effects of different factors on Co(II) adsorption

Effect of adsorbent dosage

Figure 4a shows the effect of the Sr-HAP dosage on the removal efficiency of Co(II). Three solutions with 10, 20 and 50 mg/L Co(II) were prepared for investigation. At 25 °C and pH = 5, the Co(II) removal efficiency of all solutions increased as the Sr-HAP dosage increased. At the Sr-HAP dosage of 0.5 g/50 mL, the Co(II) removal efficiencies of the three solutions reached their maxima of 99.83%, 99.70%, and 99.19%, respectively. On the contrary, as the dosage increased, the unit adsorption capacity of Co(II) gradually decreased. Increasing the dosage of Sr-HAP increased the amount of available adsorption sites, thus increasing the Co(II) removal efficiency. However, when the Sr-HAP dosage was excessive, the active sites could not be fully utilized (Xiong et al. 2022). As a result, the amount of Co(II) adsorbed by the adsorbent per unit mass was reduced. It should be noted that when the adsorbent dosage reached 0.30 g/50 mL, the Co(II) removal efficiencies were over 98% for the three solutions, which increased slightly as the

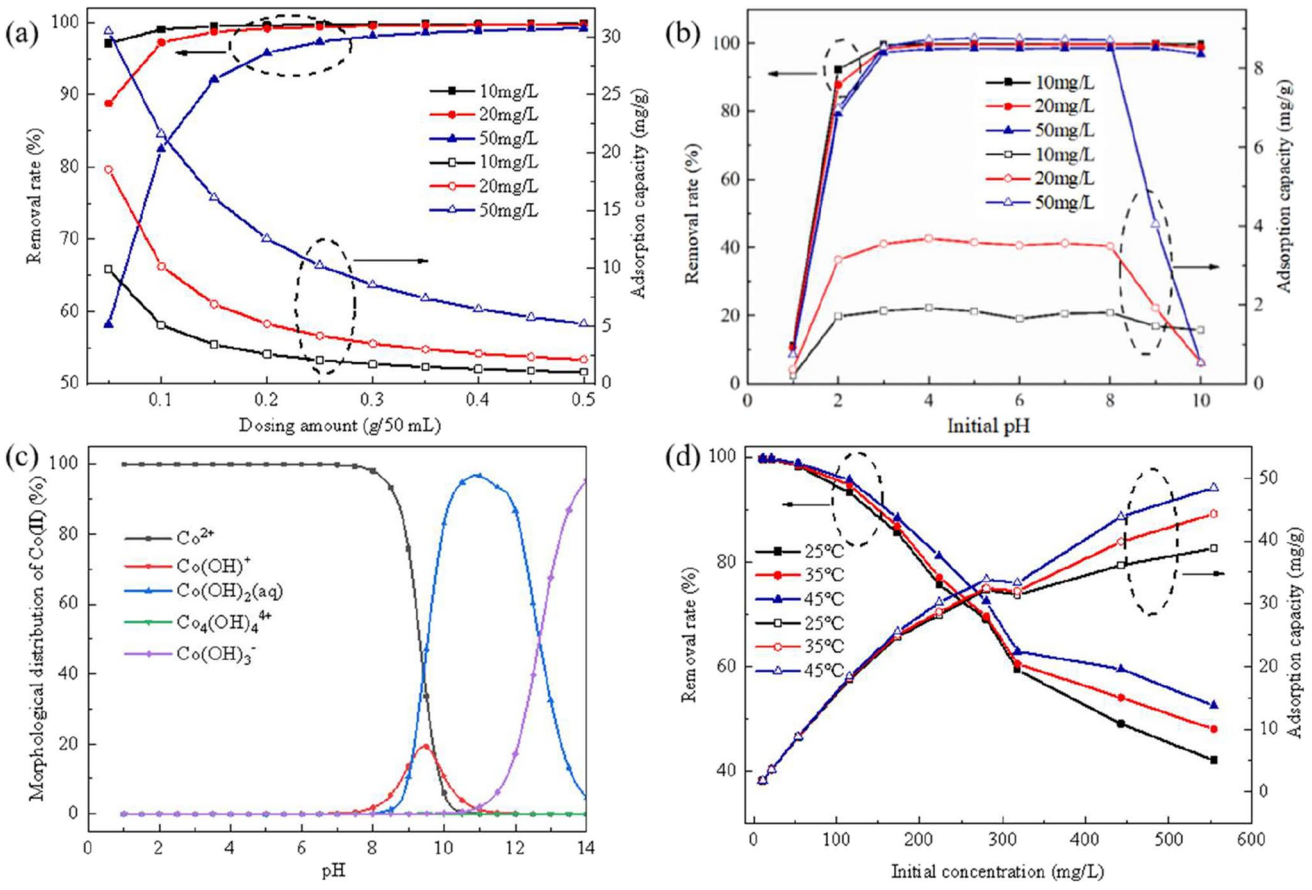

Fig. 4 Effects of different factors on Co(II) adsorption. **a** Sr-HAP dosage; **b** Initial pH; **c** Existing forms of Co ions at different pH values; **d** Initial Co(II) concentration. (fixed conditions, *V:* 50 mL, Sr-HAP dosage: 0.30 g, *T:* 25 °C, pH: 5.0, *C:* 50 mg/L)

dosage further increased to 0.50 g/50 mL. Based on this, the optimal dosage of Sr-HAP was selected as 0.30 g/50 mL.

Effect of the initial solution pH

Since Co(II) exists in different forms at different solution pH (Wu et al. 2024), solution pH is an important factor affecting the Co(II) removal. It was observed that both the removal efficiency and adsorption capacity of Co(II) were low at low pH (< 3) (Fig. 4b). When the pH value rose from 1 to 3, the Co(II) removal efficiency and adsorption capacity sharply increased and then kept constant until the solution pH increased to 8. Interestingly, when the pH further rose to 10, the Co(II) removal efficiency changed a little but the adsorption capacity significantly decreased. Under acidic conditions, Co(II) existed as a positive ion (Fig. 4c), and Sr-HAP could catch a lot of protons to be positively charged (Fig. S3). Therefore, the electrostatic repulsion between Co(II) ions and Sr-HAP led to the inferior removal. On the other hand, Sr-HAP may partially dissolve at the pH value less than 3, further limiting the Co(II) uptake. In the pH range of 4 ~ 8, the electrostatic repulsion was weak and Sr-HAP was stable. As a result, Sr-HAP showed good adsorption performance on Co(II). However, Co(II) existed in a hydroxide form when the pH value exceeded 8 and might be partially removed in the form of precipitate rather than direct adsorption by Sr-HAP under alkaline conditions. Therefore, the Co(II) removal efficiency remained basically unchanged while the adsorption capacity by Sr-HAP suddenly dropped. It should be noted that for the solutions with 10, 20, and 50 mg/L Co(II), the removal efficiency of Co(II) was above 98.3% when the pH value was greater than 3. These results revealed that Sr-HAP could be used to effectively remove Co(II) in a wide pH range.

Effect of initial Co(II) concentration and temperature

Figure 4d shows the effects of different initial Co(II) concentrations and temperatures on Co(II) adsorption. It can be seen that the removal efficiency of Co(II) gradually decreased as the initial Co(II) concentration increased, but the Co(II) adsorption capacity of Sr-HAP increased. When the Sr-HAP dosage was fixed, the total number of active sites for adsorbing Co(II) was limited. As the amount of Co(II) increased, a lot of Co(II) could not be adsorbed, leading to a decrease in the removal efficiency (Sadeghizadeh et al. 2019; Yan et al. 2014). However, the active sites on the Sr-HAP's surface were fully occupied when they were exposed to excessive Co(II). As a result, the unit adsorption amount (adsorption capacity) of Co(II) by Sr-HAP was increased. At a certain Co(II) concentration, both the removal efficiency and adsorption capacity increased as the temperature increased. For example, they were 42.03% and 38.795 mg/g at 25 °C, respectively, which increased to 52.47% and 48.467 mg/g, respectively, as the temperature increased to 45 °C. This might be because the adsorption of Co(II) by Sr-HAP was an endothermic process and increasing temperature was favorable to the Co(II) removal. The adsorption capacity of Sr-HAP was compared with those of other reported adsorbents, and the results are listed in Table S1. The results showed that although the adsorption capacity of Sr-HAP was not the highest, it performed better than most reported adsorbents, indicating that Sr-HAP was a good candidate for removing Co(II) from wastewater.

Adsorption kinetics

Various kinetic models, such as pseudo-first-order and pseudo-second-order kinetic models, Elovich, and intraparticle diffusion models were used to fit the adsorption data in Fig. S4. The description of different models were presented in the Supplementary Material. The results in Fig. 5a–c and Table 1 shows that compared with the pseudo-first-order and Elovich models, the pseudo-second order kinetic model fitted the adsorption data well with good correlation coefficients (the values of R^2 were close to 1). This suggested that the pseudo-second order kinetic model was suitable for describing the Co(II) adsorption process, which was a chemisorption process. At 25, 35 and 45 °C, the theoretical equilibrium adsorption amounts calculated by the pseudo-second-order model were 15.789, 15.974, and 16.181 mg/g, respectively, which were in good agreement with the experimental data. Based on the kinetic constants (K_2), the activation energy (E_a) of Co(II) adsorption was calculated by using the Arrhenius equation (the data were plot in Fig. S5). Generally, physical adsorption is easy to occur and its activation energy does not exceed 4.2 kJ/mol, while chemisorption requires more energy as a driving force and the associated activation energy ranges between 8.4 ~ 83.7 kJ/mol (Aksu 2002). According to the result in Fig. S5, the value of E_a was 11.157 kJ/mol, which further demonstrated that Co(II) adsorption onto Sr-HAP was a chemisorption process.

As shown in Fig. 5d, the adsorption data are also fitted well by the internal diffusion model. According to the fitting results, the adsorption of Co(II) could be divided into three stages, and the fitting parameters are listed in Table 2. The first stage was external diffusion, in which the diffusion coefficients (K_{d1}) were high, indicating the rapid diffusion of Co(II) to the Sr-HAP's surface. In this case, the sudden increase of the removal efficiency occurred in the initial period. When the Co(II) ions reached the outer surface of Sr-HAP, they migrated into the pores of Sr-HAP via internal diffusion with relatively low diffusion rate (the values of K_{d2} were relatively low). Finally, Co(II) ions were adsorbed tardily onto the Sr-HAP adsorbent and eventually realized adsorption-desorption equilibrium.

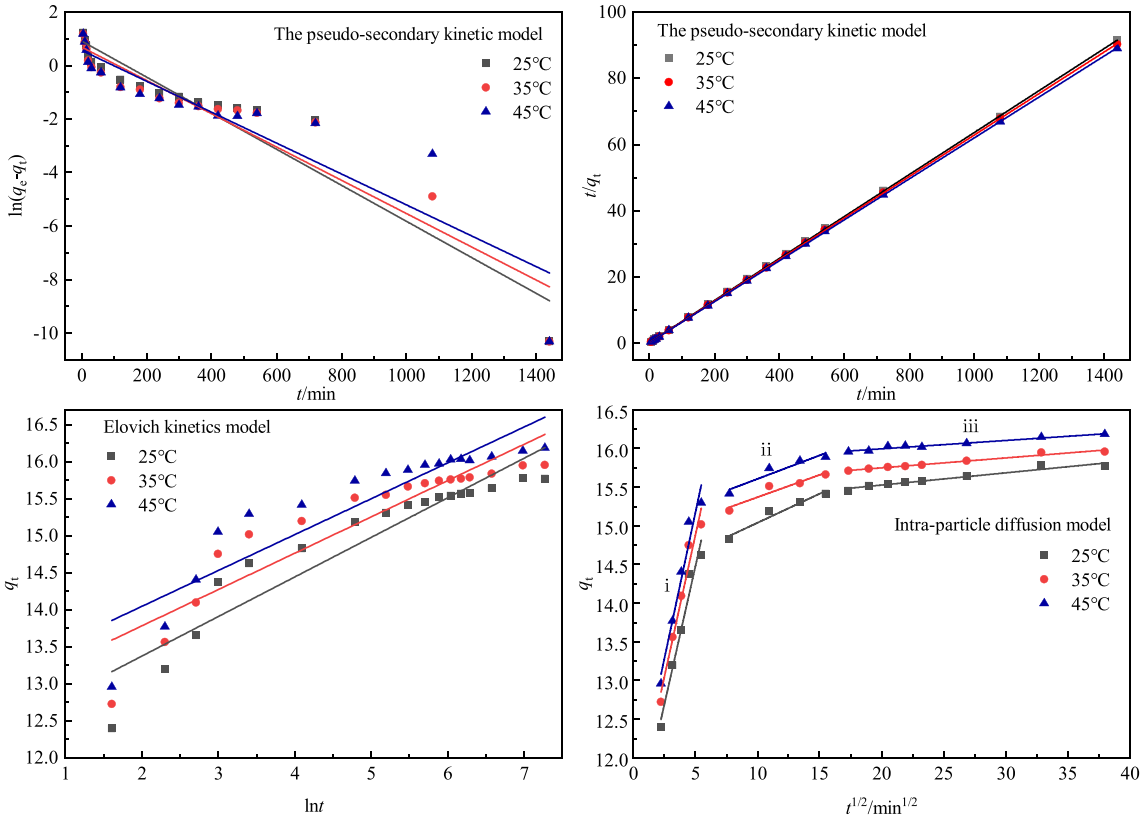

Fig. 5 Kinetic model fitting of Co(II) adsorption (*C*: 100 mg·L^{-1}, *V:* 50 mL, Sr-HAP dosage: 0.30 g, pH: 5.0)

Table 1 Kinetic fitting parameters of Co(II) adsorption

Model	*T*/°C	Rate constant, K_1 (/min) or K_2 (g/(mg·min))	*Qe, cal* (mg/g)	*qe, exp* (mg/g)	R^2
pseudo-first-order kinetic model	25	0.0067	2.491	15.767	0.9094
	35	0.0062	1.987	15.955	0.8984
	45	0.0058	1.759	16.181	0.8379
pseudo-second-order kinetic model	25	0.0147	15.798	15.767	1
	35	0.0177	15.974	15.955	1
	45	0.0195	16.181	16.181	1
Elovich kinetic model	25				0.8863
	35				0.8490
	45				0.8346

Table 2 Parameters of the internal diffusion model for Co(II) adsorption

T/°C	K_{d1}	C_1 (mg/g)	R^2	K_{d2}	C_2 (mg/g)	R^2	K_{d3}	C_3 (mg/g)	R^2
25	0.715	10.90	0.981	0.075	14.29	0.977	0.016	15.2102	0.971
35	0.734		0.981	0.058		0.957	0.013	15.493	0.985
45	0.756		0.978	0.061		0.955	0.011	15.779	0.979

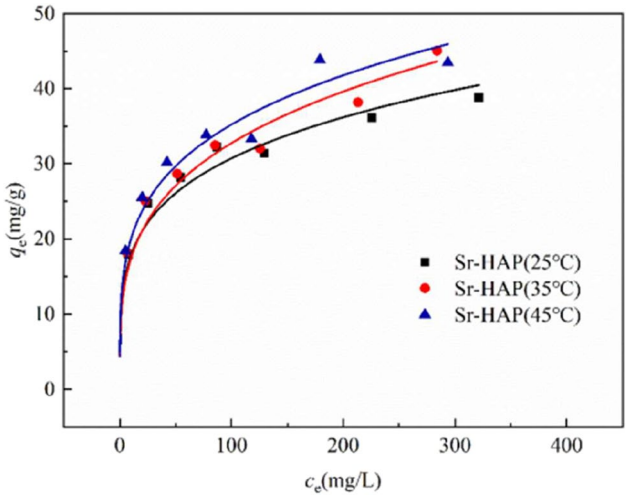

Fig. 6 Isothermal adsorption curves of Co(II) (*V:* 50 mL, Sr-HAP dosage: 0.30 g, pH: 5.0)

The above analysis revealed that the second and the third stages (internal diffusion and surface adsorption) were the rate-controlled steps of Co(II) adsorption.

Adsorption isotherms

The isothermal adsorption curves of Co(II) at different temperatures are shown in Fig. 6. For a specific temperature, the adsorption capacity (q_e) of Sr-HAP rose with the increase in the Co(II) equilibrium concentration (c_e). However, the rising tendency decelerated at the relatively high c_e value due to the limited active sites of Sr-HAP for Co(II). Under the same c_e value, Sr-HAP had larger adsorption capacity at higher temperature. This was consistent with the results in Fig. 4d, in which the adsorption of Co(II) was promoted by increasing temperature.

The isothermal adsorption data were fitted by the Langmuir and Freundlich models (the description was given in the Supplementary Material). As shown in Fig. 7 and Table 3, by and large, both Langmuir and Freundlich models could fit the data well with high correlation coefficients ($R^2 > 0.98$). However, the Langmuir model fitted the data better than the Freundlich model at lower Co(II) equilibrium concentration, while the opposite was true at higher Co(II) equilibrium concentration. As known, the Langmuir model describes the homogeneous surface adsorption of an adsorbent (monolayer adsorption), while the Freundlich model describes the heterogeneous adsorption (multilayer adsorption) (Tran et al. 2017). According to the Langmuir theory, it could be assumed that the Sr-HAP adsorbent had uniformly distributed and single-layer surface adsorption sites, which played the role of monolayer adsorption for Co(II) under the relatively low Co(II) equilibrium concentration. At this point, the adsorbed Co(II) underwent ion exchange with Ca(II) and Sr(II) on the Sr-HAP's surface. At the high Co(II) equilibrium concentration, in addition to the ion exchange, surface complexation might also occur. When Co(II) ions passed through the Sr-HAP's surface, the complex of $(Sr\text{-}HAP\text{-}O)_2$-Co would form, leading to the heterogeneous adsorption of Co(II) (Zhang et al. 2021). Herein, the values of separation factor (R_L) at different temperatures obtained from the Langmuir model were between 0 and 1,

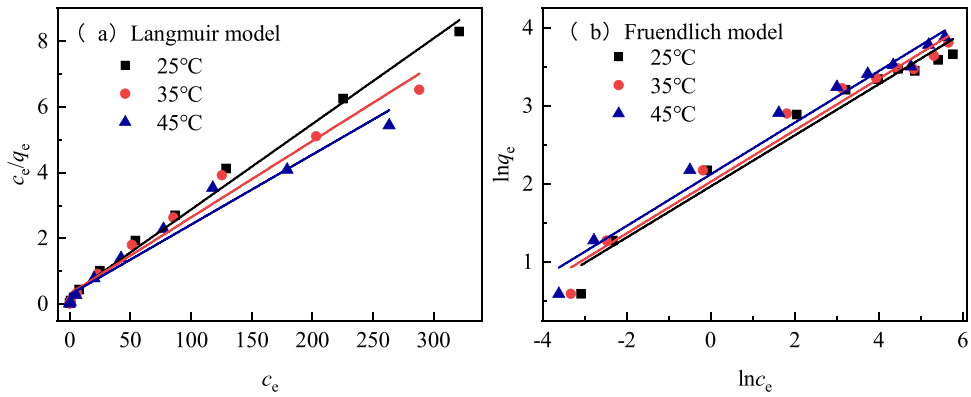

Fig. 7 **a** Langmuir and **b** Fruendlich isothermal models for Co(II) adsorption

Table 3 Fitting parameters of Langmuir and Fruendlich isothermal models

T/°C	Langmuir model				Freundlich model		
	q_m/(mg/g)	K_L/(L/mg)	R_L	R^2	K_F/[mg^{1-n}/(g·L^n)]	1/n	R^2
25	38.462	0.096	0.020 ~ 0.511	0.996	7.156	0.327	0.982
35	43.103	0.074	0.026 ~ 0.576	0.988	7.587	0.330	0.985
45	46.948	0.074	0.026 ~ 0.575	0.983	8.354	0.331	0.987

and the strength increase factor of adsorption capacity ($1/n$) obtained from the Freundlich model was lees than 1, indicating that Sr-HAP had good adsorption properties for Co(II) (Long et al. 2019; Zendehdel et al. 2022).

Thermodynamic studies

Based on the adsorption equilibrium constant at different temperatures, three thermodynamic parameters, namely, Gibbs free energy (ΔG^{θ}), enthalpy (ΔH^{θ}), and entropy (ΔS^{θ}), were calculated to determine the thermodynamic characteristics of Co(II) adsorption by Sr-HAP. The calculation method can be referred to the Supplementary Material. At different temperatures, the ΔG^{θ} values were less than zero (Table 4), indicating that Co(II) adsorption by Sr-HAP was spontaneous (Staroń et al. 2017). The ΔG^{θ} value decreased as the temperature increased, suggesting that increasing temperature favored the spontaneous Co(II) adsorption process. The adsorption enthalpy (ΔH^{θ}) was positive, which indicated that the Co(II) adsorption process was endothermic and increasing temperature was beneficial for Co(II) adsorption. This was in agreement with the results in Figs. 4d and 6, in which the adsorption amount of Co(II) increased with increasing temperature. The value of ΔS^{θ} was small but positive, indicating that the disorder of the solid-liquid interface increased as the adsorption proceeded. This was likely related to the structural change of Sr-HAP caused by the chemical interactions (chemisorption, ion exchange, and surface complexation) between Sr-HAP and Co(II) species. Similar results were also reported in previous studies (Mo et al. 2020; Mondal et al. 2022).

Table 4 Thermodynamic parameters of Co(II) adsorption

T/°C	ΔG^{θ}/(J/mol)	ΔH^{θ}/(J/mol)	ΔS^{θ}/J/(mol·K)
25	−6087.0157	14,904.5078	70.4413
35	−6791.4292		
45	−7495.8428		

Cycling performance of Sr-HAP

Co(II) desorption from Sr-HAP by using different compounds as desorption reagents was investigated, the results are shown in Fig. 8. It was difficult for Co(II) to to be desorbed from the Sr-HAP adsorbent in neutral or alkaline H_2O, NaCl, $NaHCO_3$, and NaOH solutions. In contrast, Co(II) ions were easily released from Sr-HAP in acidic TCLP, EDTA, HCl, $ZnCl_2$, and $CaCl_2$ solutions. These results were likely related to that in acidic environment, the large amount of H^+ inhibited the chemical reaction of Co(II) on the surface of Sr-HAP, such as surface complexation, resulting in the release of Co(II) from Sr-HAP. Aided by the acidic desorption reagent (taking EDTA as an example), the removal rate of Co(II) by Sr-HAP was still more than 81.55% at the third cycle (Fig. S6), indicating that Sr-HAP could be repeatedly used for removing Co(II) from wastewater.

Adsorption mechanism

According to the characterization results, the Co(II) removal process by Sr-HAP may have involved chemisorption, ion

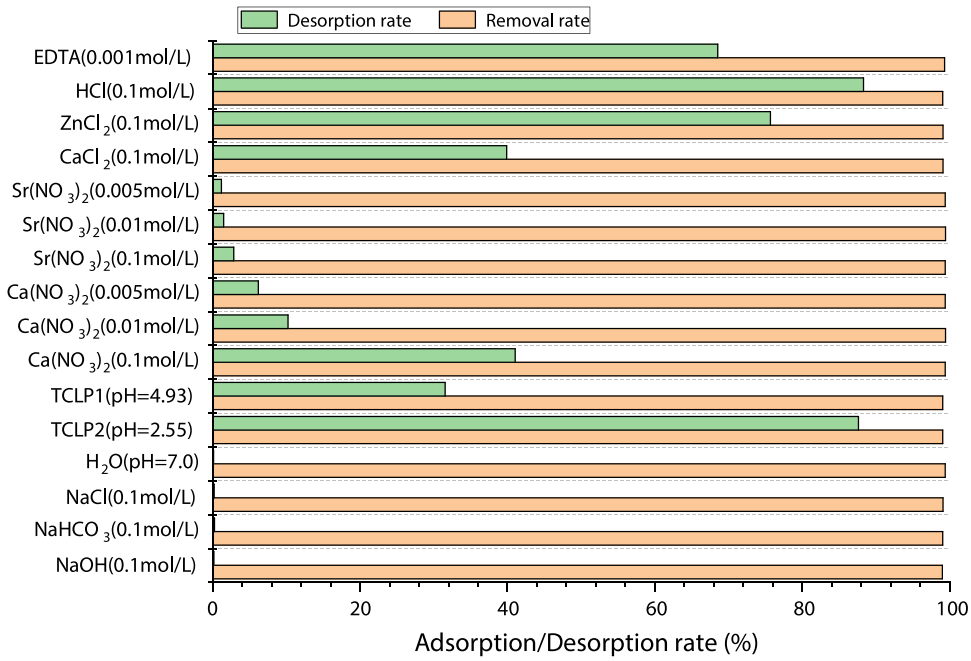

Fig. 8 Desorption rates of Co(II) from Sr-HAP with different desorption regents

exchange and surface complexation (Chen et al. 2021; Wei et al. 2021). To further understand the adsorption mechanism of Co(II) by Sr-HAP, the solution pH, Co(II) adsorption amount, and the total release amount of Ca(II) and Sr(II) were explored under different initial Co(II) concentrations. Figure 9 shows that when Co(II) ions were adsorbed, Ca(II) and Sr(II) ions were synchronously released to the solution, indicating that ion exchange occurred between Co(II) and Ca(II) or Sr(II) (Eq. 1). However, the total released amount of Ca(II) and Sr(II) was greater than the adsorption amount of Co(II), indicating that in addition to the ion exchange mechanism, other mechanisms may exist. Moreover, the higher the initial concentration of Co(II), the lower the final solution pH. That was to say, the increasing amount of Co(II) adsorbed onto Sr-HAP resulted in the decrease in the final solution pH. This was likely to that Co(II) ions combined with the O atoms of hydroxyl groups on the Sr-HAP's surface to displace the H atoms, enabling H^+ ions to be released to the solution and then increasing the solution acidity (Eqs. 2–3). Therefore, surface complexation reactions also occurred during the Co(II) removal process (Zeng et al. 2022). In a word, Sr-HAP could effectively remove Co(II) ions from water via chemisorption, ion exchange and surface complexation.

$$Sr_5Ca_5(PO_4)_6(OH)_2 + (x+y)Co^{2+} \rightarrow (5-x)Sr^{2+} + (5-y)Ca^{2+} + Sr_xCa_yCo(x+y)(PO_4)_6(OH)_2 \quad (1)$$

$$Sr-HAP-OH + Co^{2+}{}_{(aq)} \leftrightarrow Sr-HAP-O-Co^{+} + H^{+}{}_{(aq)} \quad (2)$$

$$2Sr-HAP-OH + Co^{2+}{}_{(aq)} \leftrightarrow (Sr-HAP-O)_2-Co + 2H^{+}{}_{(aq)} \quad (3)$$

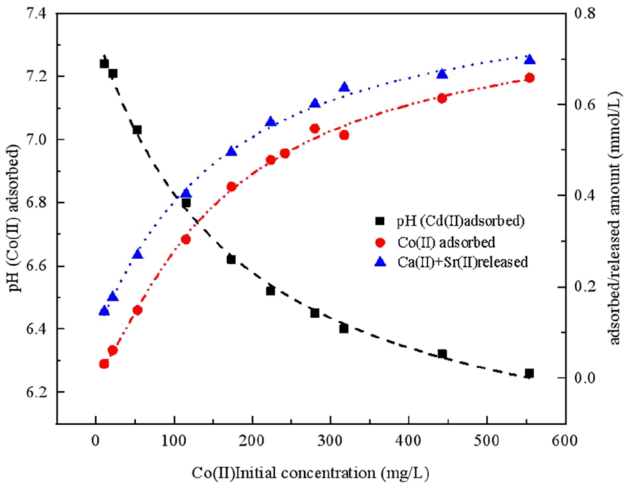

Fig. 9 Final solution pH, the Co(II) adsorption amount and the total release amount of Ca(II) and Sr(II) under different initial Co(II) concentrations (*T:* 25 °C, pH_0: 5.0)

Conclusions

This study synthesized an efficient Sr-doped HAP (Sr-HAP) adsorbent for removing Co(II) ions from water. Experimental results showed that the Sr-HAP adsorbent had effective Co(II) adsorption performance. When the Sr-HAP dosage was 0.30 g/50 mL, solution pH was 5, initial Co(II) concentration was 50 mg/L, and temperature was 25–45 °C, the Co(II) removal efficiency reached more than 98%. In addition, Sr-HAP could effectively adsorb Co(II) in a wide pH range of 3–8. The adsorption of Co(II) ions by Sr-HAP was described well by the pseudo-second-order kinetic model, indicating Co(II) adsorption was a chemisorption process. At lower Co(II) equilibrium concentration, the Langmuir model could fit the data better than the Freundlich model but opposite at higher Co(II) equilibrium concentration, revealing that the adsorption of Co(II) changed from monolayer adsorption to multilayer adsorption as the Co(II) equilibrium concentration increased. The internal diffusion and surface adsorption were the rate-controlled steps of Co(II) adsorption. Thermodynamic study demonstrated that the adsorption process of Co(II) was spontaneous and endothermic, and increasing temperature was conducive to the adsorption. The mechanism analysis revealed that in addition to chemisorption, ion exchange and surface complexation also played vital roles in the Co(II) removal.

Supplementary Information The online version contains supplementary material available at https://doi.org/10.1007/s11356-024-33239-4.

Author contribution Zongqiang Zhu: Conceptualization, Methodology, Funding acquisition.
Shuangshuang Liu: Data curation, Writing—Original Draft.
Yinian Zhu: Methodology, Project administration.
Hao He: Investigation, Data curation.
Jun Zhang: Data curation.
Xiaoxin Mo: Data curation.
Shen Tang: Formal analysis, Data curation.
Yinming Fan: Supervision, Validation.
Lihao Zhang: Supervision, Data curation.
Zhou Xiaobin: Conceptualization, Supervision, Writing—Review & Editing.

Funding This work was financially supported by the National Natural Science Foundation of China (Nos. 51978188, 42267027, 42063003), the Chinese Postdoctoral Science Foundation (2019M650869).

Data availability All data that support the findings of this study are available from the corresponding author upon reasonable request.

Declarations

Ethical approval Not applicable.

Consent to participate The author agrees to participate.

Consent to publish The author agrees to publish the article.

Competing interests The authors declare no competing interests.

References

Aksu Z (2002) Determination of the equilibrium, kinetic and thermodynamic parameters of the batch biosorption of nickel(II) ions onto *Chlorella vulgaris*. Process Biochem 38:89–99. https://doi.org/10.1016/S0032-9592(02)00051-1

ALOthman Z (2012) A review: fundamental aspects of silicate mesoporous materials. Materials 5:2874–2902. https://doi.org/10.3390/ma5122874

Bhawna M, Kirandeep KS (2023) Occurrence and impact of heavy metals on environment. Mater Today: Proc. https://doi.org/10.1016/j.matpr.2023.01.317

Campisi S, Evangelisti C, Postole G, Gervasini A (2021) Combination of interfacial reduction of hexavalent chromium and trivalent chromium immobilization on tin-functionalized hydroxyapatite materials. Appl Surf Sci 539:148227. https://doi.org/10.1016/j.apsusc.2020.148227

Chakraborty R, Asthana A, Singh AK, Jain B, Susan ABH (2022) Adsorption of heavy metal ions by various low-cost adsorbents: a review. Int J Environ an Ch 102:342–379. https://doi.org/10.1080/03067319.2020.1722811

Che N, Liu N, Li Y, Li C, Liu Y, Li CL (2022) Three dimensional BC/rGA aerogel: preparation, characterization, and adsorption of Cr(VI). Biochar 4:65. https://doi.org/10.1007/s42773-022-00191-w

Chen H, Wang MQ, Yu Y, Liu H, Lu S-Y, Bao S-J, Xu M (2017) Assembling hollow cobalt sulfide nanocages array on graphene-like manganese dioxide nanosheets for superior electrochemical capacitors. ACS Appl Mater Interfaces 9:35040–35047. https://doi.org/10.1021/acsami.7b12069

Chen YN, Li ML, Li YP, Liu YH, Chen YR, Li H, Li LSZ, Xu FT, Jiang HJ, Chen L (2021) Hydroxyapatite modified sludge-based biochar for the adsorption of Cu^{2+} and Cd^{2+}: adsorption behavior and mechanisms. Bioresource Technol 321:124413. https://doi.org/10.1016/j.biortech.2020.124413

Cherif A, Alzahrani AYA, Hammoudan I, Saddik R, Tighadouini S (2023) Synthesis of imidazothiazole Schiff base functionalized silica as an adsorbent for efficient and selective removal of Cu(II) from wastewater: a combined experimental and theoretical investigation. Mater Today Sustain 24:100508. https://doi.org/10.1016/j.mtsust.2023.100508

Deliyanni EA, Nalbandian L, Matis KA (2006) Adsorptive removal of arsenites by a nanocrystalline hybrid surfactant–akaganeite sorbent. J Colloid Interf Sci 302:458–466. https://doi.org/10.1016/j.jcis.2006.07.007

Hokkanen S, Repo E, Westholm LJ, Lou S, Sainio T, Sillanpää M (2014) Adsorption of Ni^{2+}, Cd^{2+}, PO_4^{3-} and NO_3^- from aqueous solutions by nanostructured microfibrillated cellulose modified with carbonated hydroxyapatite. Chem Eng J 252:64–74. https://doi.org/10.1016/j.cej.2014.04.101

Iconaru S, Motelica-Heino M, Guegan R, Beuran M, Costescu A, Predoi D (2018) Adsorption of Pb(II) ions onto hydroxyapatite nanopowders in aqueous solutions. Materials 11:2204. https://doi.org/10.3390/ma11112204

Joo S, Shim H-W, Choi J-J, Lee C-G, Kim D-G (2020) A method of synthesizing lithium hydroxide nanoparticles using lithium sulfate from spent batteries by 2-step precipitation method. Korean J Met Mater 58:286–291. https://doi.org/10.3365/KJMM.2020.58.4.286

Kosiorek M (2019) Effect of cobalt on the environment and living organisms-a review. Appl Ecol Env Res. https://doi.org/10.15666/aeer/1705_1141911449

Leyva AG, Marrero J, Smichowski P, Cicerone D (2001) Sorption of antimony onto hydroxyapatite. Environ Sci Technol 35:3669–3675. https://doi.org/10.1021/es0009929

Li H, Li Z, Sun M, Wu Z, Shen W, Fu YQ (2019) Zinc cobalt sulfide nanoparticles as high performance electrode material for asymmetric supercapacitor. Electrochim Acta 319:716–726. https://doi.org/10.1016/j.electacta.2019.07.033

Li M, Yuan G, Zeng Y, Peng H, Yang Y, Liao J, Yang J, Liu N (2021) Efficient removal of Co(II) from aqueous solution by flexible metal-organic framework membranes. J Mol Liq 324:114718. https://doi.org/10.1016/j.molliq.2020.114718

Li Z, Zhang W, Liu X, Wang X, Dai H, Chen F, Tang Y, Li J (2023) Iron-Cobalt magnetic porous carbon beads activated peroxymonosulfate for enhanced degradation and Microbial inactivation. J Colloid Interf Sci 652:1878–1888. https://doi.org/10.1016/j.jcis.2023.09.018

Liao J, Xiong T, Ding L, Xie Y, Zhang Y, Zhu W (2022) Design of a renewable hydroxyapatite-biocarbon composite for the removal of uranium(VI) with high-efficiency adsorption performance. Biochar 4:29. https://doi.org/10.1007/s42773-022-00154-1

Liu Z, Chen L, Zhang Z, Li Y, Dong Y, Sun Y (2013) Synthesis of multi-walled carbon nanotube–hydroxyapatite composites and its application in the sorption of Co(II) from aqueous solutions. J Mol Liq 179:46–53. https://doi.org/10.1016/j.molliq.2012.12.011

Long Y, Jiang J, Hu J, Hu X, Yang Q, Zhou S (2019) Removal of Pb(II) from aqueous solution by hydroxyapatite/carbon composite: Preparation and adsorption behavior. Colloid Surf A 577:471–479. https://doi.org/10.1016/j.colsurfa.2019.06.011

Mahar H, Soomro SA, Memon AR (2023) Raw and modified pakistani kaolin as an efficient adsorbent for the removal of arsenic from groundwater. Phys Chem Earth 131:103442. https://doi.org/10.1016/j.pce.2023.103442

Mao M, Yan T, Shen J, Zhang J, Zhang D (2021) Capacitive removal of heavy metal ions from wastewater *via* an electro-adsorption and electro-reaction coupling process. Environ Sci Technol 55:3333–3340. https://doi.org/10.1021/acs.est.0c07849

Metwally SS, Ahmed IM, Rizk HE (2017) Modification of hydroxyapatite for removal of cesium and strontium ions from aqueous solution. J Alloy Compd 709:438–444. https://doi.org/10.1016/j.jallcom.2017.03.156

Mo N, Zhu Z, Zhu Y, Liu Y, Wang X, Yang H, Zhao N (2020) Purification behavior of Zn(II) in water by magnesium hydroxyapatite: Surface complexation, and dissolution–precipitation. Int J Env Res Pub He 17:3804. https://doi.org/10.3390/ijerph17113804

Mondal A, Arora M, Dubey BK, Mumford K (2022) Comparative assessment of the characteristics and Cr(VI) removal activity of the bimetallic Fe/Cu nanoparticles pre- and post-coated with carboxymethyl cellulose. Chem Eng J 444:136343. https://doi.org/10.1016/j.cej.2022.136343

Pourshadlou S, Mobasherpour I, Majidian H, Salahi E (2023) Facile preparation of bentonite/nano-gamma alumina composite as a cost-effective adsorbent for Ca^{2+} removal from aqueous solutions. J Ind Eng Chem 127:496–508. https://doi.org/10.1016/j.jiec.2023.07.035

Punia P, Bharti MK, Dhar R, Thakur P, Thakur A (2022) Recent advances in detection and removal of heavy metals from contaminated water. ChemBioEng Rev 9:351–369. https://doi.org/10.1002/cben.202100053

Sadeghizadeh A, Ebrahimi F, Heydari M, Tahmasebikohyani M, Ebrahimi F, Sadeghizadeh A (2019) Adsorptive removal of Pb(II) by means of hydroxyapatite/chitosan nanocomposite hybrid nanoadsorbent: ANFIS modeling and experimental study. J Environ Manage 232:342–353. https://doi.org/10.1016/j.jenvman.2018.11.047

Shamrai VF, Karpikhin AE, Sirotinkin VP, Kalita VI, Komlev DI (2014) Evolution of the calcium hydroxyapatite crystal structure under plasma deposition and subsequent reducing treatment. Crystallogr Rep+ 59:179–185. https://doi.org/10.1134/S1063774514020205

Singh G, Saini A, Pabla BS (2023) Preparation and characterization of Sr-doped HAp biomedical coatings on polydopamine-treated Ti6Al4V substrates. Surf Rev Lett 30:2141009. https://doi.org/10.1142/S0218625X21410092

Staroń P, Chwastowski J, Banach M (2017) Sorption and desorption studies on silver ions from aqueous solution by coconut fiber. J Clean Prod 149:290–301. https://doi.org/10.1016/j.jclepro.2017.02.116

Tran HN, You S-J, Hosseini-Bandegharaei A, Chao H-P (2017) Mistakes and inconsistencies regarding adsorption of contaminants from aqueous solutions: a critical review. Water Res 120:88–116. https://doi.org/10.1016/j.watres.2017.04.014

Wei W, Li J, Han X, Yao Y, Zhao W, Han R, Li S, Zhang Y, Zheng C (2021) Insights into the adsorption mechanism of tannic acid by a green synthesized nano-hydroxyapatite and its effect on aqueous Cu(II) removal. Sci Total Environ 778:146189. https://doi.org/10.1016/j.scitotenv.2021.146189

Wu X, Wang Z, Shao G, Qin B, Wang Y, Wang T, Liu Z, Fu Y (2024) Supramolecular cellulose-based heavy metal adsorbent for efficient and accurate removal of cobalt (II) for water treatment. React Funct Polym 194:105759. https://doi.org/10.1016/j.reactfunctpolym.2023.105759

Xiong T, Li Q, Liao J, Zhang Y, Zhu W (2022) Highly enhanced adsorption performance to uranium(VI) by facile synthesized hydroxyapatite aerogel. J Hazard Mater 423:127184. https://doi.org/10.1016/j.jhazmat.2021.127184

Yan Y, Dong X, Sun X, Sun X, Li J, Shen J, Han W, Liu X, Wang L (2014) Conversion of waste FGD gypsum into hydroxyapatite for removal of Pb^{2+} and Cd^{2+} from wastewater. J Colloid Interf Sci 429:68–76. https://doi.org/10.1016/j.jcis.2014.05.010

Zendehdel M, Rezaeian K, Rezaei A, Jalalvandi S (2022) Synthesis and characterization of a low-cost and eco-friendly hydroxyapatite/clinoptilolite/NH_2 adsorbent for simultaneous removal of Cr(VI) and F^-. SILICON 14:8643–8659. https://doi.org/10.1007/s12633-021-01649-5

Zeng Y, Yuan G, Lan T, Li F, Yang J, Liao J, Yang Y, Liu N (2022) Synthesis and application of zirconium phosphate mesoporous coordination polymer for effective removal of Co(II) from aqueous solutions. Nucl Eng Technol 54:4013–4021. https://doi.org/10.1016/j.net.2022.06.013

Zhang Y, Cao N, Szunerits S, Addad A, Roussel P, Boukherroub R (2019) Fabrication of ZnCoS nanomaterial for high energy flexible asymmetric supercapacitors. Chem Eng J 374:347–358. https://doi.org/10.1016/j.cej.2019.05.181

Zhang M, Gu P, Yan S, Liu Y, Zhang G (2021) Effective removal of radioactive cobalt from aqueous solution by a layered metal sulfide adsorbent: mechanism, adsorption performance, and practical application. Sep Purif Technol 256:117775. https://doi.org/10.1016/j.seppur.2020.117775

Zhong H, Campos-Roldán C, Zhao Y, Zhang S, Feng Y, Alonso-Vante N (2018) Recent advances of cobalt-based electrocatalysts for oxygen electrode reactions and hydrogen evolution reaction. Catalysts 8:559. https://doi.org/10.3390/catal8110559

Zhu Y, Jiang Y, Zhu Z, Deng H, Ding H, Li Y, Zhang L, Lin J (2018) Preparation of a porous hydroxyapatite-carbon composite with the bio-template of sugarcane top stems and its use for the Pb(II) removal. J Clean Prod 187:650–661. https://doi.org/10.1016/j.jclepro.2018.03.275

Zhu Z, Yang Y, Fan Y, Zhang L, Tang S, Zhu Y, Zhou X (2022) Strontium-doped hydroxyapatite as an efficient adsorbent for Cd(II) removal from wastewater: performance, kinetics, and mechanism. Environ Technol Inno 28:102575. https://doi.org/10.1016/j.eti.2022.102575